Navigating the Storm: Assessing the Impact of Geomagnetic Disturbances on Low-Cost GNSS Permanent Stations

*remote sensing*

MDPI

*Article*

# Navigating the Storm: Assessing the Impact of Geomagnetic Disturbances on Low-Cost GNSS Permanent Stations

**Milad Bagheri * and Paolo Dabove**

Department of Environment, Land and Infrastructure Engineering (DIATI), Politecnico di Torino, Corso Duca degli Abruzzi 24, 10129 Turin, Italy; paolo.dabove@polito.it

* Correspondence: milad.bagheri@polito.it

**Abstract**

As contemporary society and the global economy become increasingly dependent on satellite-based systems, the need for reliable and resilient positioning, navigation, and timing (PNT) services has never been more critical. This study investigates the impact of the geomagnetic storm that occurred in May 2024 on the performance of global navigation satellite system (GNSS) low-cost permanent stations. The research evaluates the influence of ionospheric disturbances on both positioning performance and raw GNSS observations. Two days were analyzed: 8 May 2024 (DOY 129), representing quiet ionospheric conditions, and 11 May 2024 (DOY 132), coinciding with the peak of the geomagnetic storm. Precise Point Positioning (PPP) and static relative positioning techniques were applied to data from a low-cost GNSS station (DYVA), supported by comparative analysis using a nearby geodetic-grade station (TRDS00NOR). The results showed that while RMS positioning errors remained relatively stable over 24 h, the maximum errors increased significantly during the storm, with the 3D positioning error nearly doubling on DOY 132. Short-term analysis revealed even larger disturbances, particularly in the vertical component, which reached up to 3.39 m. Relative positioning analysis confirmed the vulnerability of single-frequency (L1) solutions to ionospheric disturbances, whereas dual-frequency (L1+L2) configurations substantially mitigated errors, highlighting the effectiveness of ionosphere-free combinations during storm events. In the second phase, raw GNSS observation quality was assessed using detrended GPS L1 carrier-phase residuals and signal strength metrics. The analysis revealed increased phase instability and signal degradation on DOY 132, with visible cycle slips occurring between epochs 19 and 21. Furthermore, the average signal-to-noise ratio (SNR) decreased by approximately 13% for satellites in the northwest sky sector, and a 5% rise in total cycle slips was recorded compared with the quiet day. These indicators confirm the elevated measurement noise and signal disruption associated with geomagnetic activity. These findings provide a quantitative assessment of low-cost GNSS receiver performance under geomagnetic storm conditions. This study emphasizes their utility for densifying GNSS infrastructure, particularly in regions lacking access to geodetic-grade equipment, while also outlining the challenges posed by space weather.

**Keywords:** low-cost GNSS; geomagnetic storm; Precise Point Positioning (PPP); open-source; ionospheric disturbances



Academic Editors: Samsung Lim and Badal Pokharel

Received: 2 July 2025
Revised: 15 August 2025
Accepted: 20 August 2025
Published: 23 August 2025

**Citation:** Bagheri, M.; Dabove, P. Navigating the Storm: Assessing the Impact of Geomagnetic Disturbances on Low-Cost GNSS Permanent Stations. *Remote Sens.* **2025**, *17*, 2933. https://doi.org/10.3390/rs17172933



## 1. Introduction

Global navigation satellite systems (GNSSs) have become an essential component of contemporary society, with applications that encompass personal navigation, logistics,

scientific research, and precision agriculture. As dependence on GNSSs increases across multiple sectors, the demand for precise and dependable positioning data has risen sharply. Particularly in applications where even minor inaccuracies can result in significant consequences, such as geodetic surveying, autonomous navigation, and disaster response, it is imperative to achieve high precision in GNSS positioning. Nevertheless, the maintenance of precise GNSS positioning is a complex process dependent upon various factors, such as the quality of the receiver, atmospheric conditions, and geometry. One significant source of error in GNSS positioning is ionospheric disturbances, especially those caused by geomagnetic storms [1]. Geomagnetic storms, originating from solar wind interactions with the Earth's magnetic field, disturb the ionosphere by creating fluctuations in the density of free electrons. This results in signal refraction and scintillation, which cause delays in the signals that GNSS satellites transmit to Earth [2].

Precise Point Positioning (PPP) is a widely used high-precision GNSS method that delivers decimeter-level accuracy for individual receivers by utilizing global models and corrections, eliminating the necessity for base stations [3]. Nonetheless, PPP encounters constraints, notably prolonged convergence durations, frequently lasting several minutes, and challenges in precisely simulating atmospheric delays and ionospheric disturbances.

Numerous researchers have investigated the influence of ionospheric scintillation on the accuracy of GNSS positioning in PPP. An examination of a moderate geomagnetic storm revealed considerable accuracy degradation across 868 worldwide GNSS stations, with notable location errors particularly in the up component and South American areas [4]. A separate study investigated the impact of coronal mass ejection (CME)-induced geomagnetic storms, revealing that ionospheric disturbances heightened cycle slips and diminished positioning accuracy, especially in mid- and high-latitude areas [5]. Other research has shown severe accuracy degradation at high latitudes, with positioning errors exceeding two meters during disturbances [6], Lastly, advancements in multi-constellation GNSSs have improved PPP performance, though high-latitude regions remain vulnerable to ionospheric effects [7].

Another method for attaining high-precision GNSS positioning is the utilization of permanent GNSS networks that offer differential correction products. Networks like the International GNSS Service (IGS) [8], the European Permanent Network (EPN) [9,10], and the SPIN3 interregional positioning service [11] facilitate network real-time kinematic (NRTK) positioning by providing centimeter-level accuracy corrections for various applications. These networks are essential for facilitating scientific endeavors, encompassing the maintenance of global reference systems [12] and the observation of atmospheric delays [13]. However, deploying and maintaining GNSS stations involves significantly high costs, ranging from USD 10,000 to USD 25,000 for each piece of geodetic GNSS equipment (receiver and antenna) on a regular and uniform network, substantially limiting network expansion [14]. In response to these challenges, the development of low-cost GNSSs is a promising step forward, with complete stations (receiver and antenna) available for less than USD 400, representing only a small fraction of the cost of geodetic-grade set-ups while still enabling precise positioning. Recent research has examined the efficacy of these devices in comparison with geodetic-grade equipment in several circumstances, indicating their promise as a feasible option for applications necessitating precise positioning. Despite typically being less robust than geodetic-grade instruments, low-cost GNSS receivers have demonstrated considerable potential in delivering valuable solutions for various research and operational uses. Numerous studies have assessed the performance of low-cost GNSS devices in comparison with high-end geodetic-grade devices, emphasizing factors such as positioning accuracy, reliability, and resistance to environmental difficulties. For example research has shown that low-cost GNSS devices can offer high precision in both kinematic

and static positioning, proving valuable for atmospheric science and meteorology applications [15]. The Centipede-RTK network, for instance, has been evaluated across various fields, including water vapor monitoring [16], precision agriculture [17], and hydrographic surveys [18]. Additionally, studies have used Centipede-RTK to establish preliminary continuously operating reference station (CORS) networks to assess precise positioning [19] and measure atmospheric delays in mountainous regions [20]. Recent work further supports the use of Centipede-RTK for zenith tropospheric delay (ZTD) estimation, finding it comparable to the EUREF Permanent Network for enhancing tropospheric monitoring and climate modeling resolution [21,22]. Together, these studies illustrate that low-cost GNSS networks like Centipede-RTK hold great potential for expanding GNSS infrastructure in a cost-effective way, opening up new opportunities for precise positioning across diverse scientific and operational domains.

Building on this, the present study investigates the impact of the May 2024 extreme geomagnetic storm on positioning accuracy when low-cost receivers were deployed as master stations in a GNSS network. Specifically, this research will explore how geomagnetic disturbances influence the positioning solutions derived from low-cost receivers, evaluating both their effectiveness and limitations under such conditions. The goal is to assess whether low-cost stations can provide reliable performance during severe geomagnetic storms and identify mitigation strategies such as dual-frequency ionosphere-free combinations.

### *1.1. Geomagnetic Storms and GNSS Signals*

Geomagnetic storms are significant disruptions in the Earth's magnetosphere, typically induced by solar wind and CMEs from the sun. These storms arise from the interaction of solar particles and magnetic fields with the Earth's magnetic field, resulting in heightened ionization in the ionosphere and substantial modification of the free electron density. Such changes can significantly degrade GNSS signal quality and positioning accuracy [1].

The ionosphere, located between approximately 60 km and 1000 km above the Earth, is a key contributor to GNSS signal delays due to its high electron density. This delay is primarily a function of the total electron content (TEC), which represents the integrated electron density along the signal path. The TEC is defined as follows [3]:

$$\mathrm{TEC} = \int_{s_1}^{s_2} n_e(s)\, ds$$

where $n_e(s)$ is the electron density at point $s$ along the signal path. The TEC is typically measured in TEC units (TECUs), where 1 TECU $= 10^{16}$ electrons/m$^2$. As the TEC increases during geomagnetic storms, the GNSS signals experience larger delays and phase shifts, which introduce significant errors in positioning accuracy [23]. GNSS signals are transmitted at L-band frequencies, primarily L1 (1575.42 MHz) and L2 (1227.60 MHz). As these signals pass through the ionosphere, they are delayed by a frequency-dependent refractive index, which causes dispersion. The phase advance and group delay experienced by GNSS signals can be described as follows:

$$\Delta t = \frac{40.3 \cdot \mathrm{TEC}}{f^2}$$

where the following definitions apply:

- $\Delta t$ is the signal delay in seconds;
- TEC is the total electron content along the signal path (in TECUs);
- $f$ is the frequency of the GNSS signal in Hz.

This equation shows that the ionospheric delay is inversely proportional to the square of the frequency, meaning that higher-frequency signals (such as those for L1) experience

less delay than lower-frequency signals (like those for L2) [3]. During geomagnetic storms, as the TEC increases dramatically, this delay can become substantial, leading to phase scintillation (rapid fluctuations in signal phase) and amplitude scintillation (fluctuations in signal strength) [24]. To mitigate this delay, dual-frequency receivers can exploit the ionosphere-free combination:

$$\phi_{\mathrm{IF}} = \frac{f_1^2 \cdot \phi_1 - f_2^2 \cdot \phi_2}{f_1^2 - f_2^2}$$

where the following definitions apply:

- $\phi_{\mathrm{IF}}$ is the combined carrier-phase measurement;
- $f_1$ and $f_2$ are the L1 and L2 frequencies, respectively;
- $\phi_1$ and $\phi_2$ are the phase measurements on L1 and L2, respectively.

This ionospheric-free combination reduces the impact of ionospheric delay, making dual-frequency receivers more resilient to ionospheric conditions than single-frequency ones. However, during intense geomagnetic storms, TEC fluctuations can be severe and highly variable, introducing residual errors that can still affect dual-frequency positioning accuracy, especially in PPP applications [25].

In addition to TEC magnitude, ionospheric irregularities and scintillation are effectively captured using the Rate of TEC Index (ROTI). The ROTI quantifies rapid variations in the TEC over short time intervals and serves as a proxy for ionospheric turbulence. It is defined as the standard deviation of the rate of TEC change over time [26]:

$$\mathrm{ROTI} = \sqrt{\left\langle \left( \frac{\Delta \mathrm{TEC}}{\Delta t} \right)^2 \right\rangle - \left\langle \frac{\Delta \mathrm{TEC}}{\Delta t} \right\rangle^2}$$

where $\Delta$TEC is the difference in total electron content between successive epochs and $\Delta t$ is the temporal resolution of the measurements.

Another important parameter is the Kp index, used to quantify geomagnetic storm intensity [27]. Introduced by Julius Bartels in 1949 [28], the Kp index reflects the planetary-scale disturbance level in the Earth's magnetic field, based on observations every 3 hours from 13 geomagnetic observatories worldwide. The Kp index is routinely provided by the German Research Centre for Geosciences (GFZ, https://kp.gfz-potsdam.de/en/, accessed on 10 June 2025), which contributes this data to the International Service of Geomagnetic Indices (ISGI) of the International Association of Geomagnetism and Aeronomy (IAGA).

More recently, several interplanetary coronal mass ejections (ICMEs) reached the Earth's magnetosphere on 10 May 2024, triggering the strongest geomagnetic storm since November 2003. Figure 1 illustrates the evolution of the Kp index and the Geomagnetic Disturbance Index (Dst) from 8 to 14 May 2024, encompassing the initial, peak, and recovery phases of the storm.

As shown in Figure 1, the Kp index remained below five during the first two days of the observed period (May 8–9), indicating geomagnetically quiet-to-unsettled conditions. A rapid escalation occurred late on May 10, as several ICMEs impacted the Earth's magnetosphere, with Kp values rising above eight, classified as a G4 (severe) geomagnetic storm according to the NOAA Space Weather Scales [27]. The peak disturbance was sustained over multiple three-hour intervals between May 10 and May 11, with values briefly exceeding the threshold for a G5 (extreme) event ($K_p \geq 9$). Following the peak, the Kp index gradually declined but remained elevated (G1–G2 level) until May 13 before returning to quiet conditions by May 14.

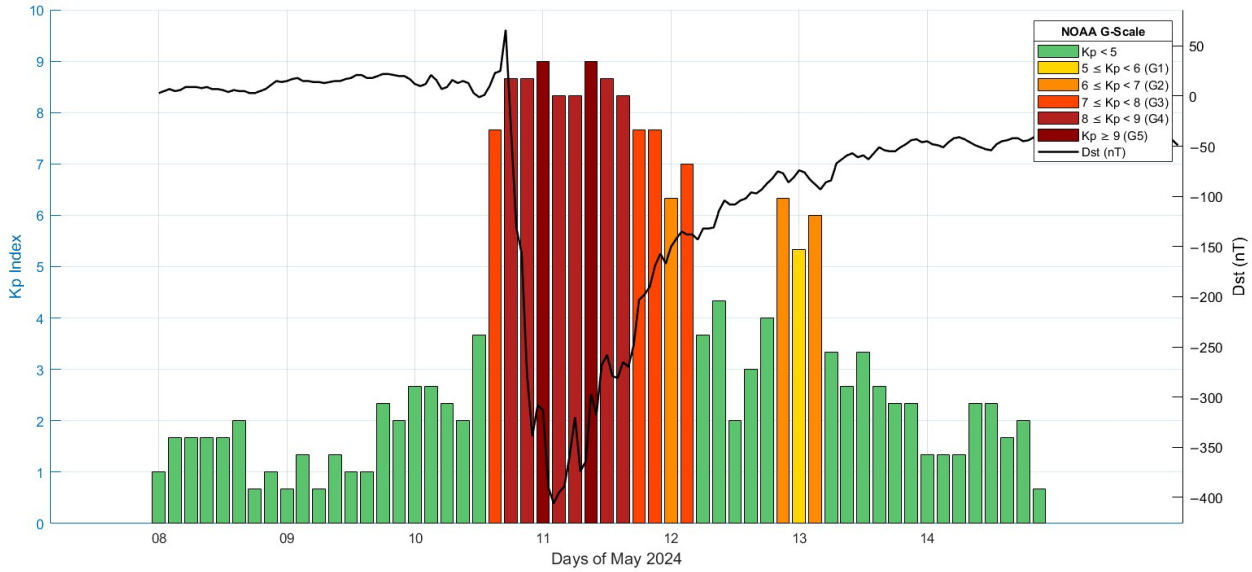


**Figure 1.** $K_p$ index (color-coded according to the NOAA Space Weather Scale for geomagnetic storms [27]) and Dst (black line) from 8 to 14 May 2024. Data obtained from GFZ (https://kp.gfz-potsdam.de/en/, accessed on 10 June 2025).

Moreover, on the same storm day (11 May 2024), regional ROTI maps over the European and Greenland sectors (Figure 2) indicated significant ionospheric disturbances, with pronounced activity over the auroral regions.

### *1.2. Research Gap and Objectives*

Prior work showed that geomagnetic storms significantly degrade PPP performance, especially at high latitudes. Linty et al. (2018) [29] reported doubled positioning errors at Svalbard during the September 2017 storm due to phase scintillation. Luo et al. (2018) [30] observed PPP errors exceeding 1 m at high latitudes during super storms, with ROTI maps linking ionospheric disturbances to higher GPS errors and cycle slip rates. Dabove et al. (2020) [7] demonstrated robustness gains for PPP solutions during disturbed ionospheric periods, improving both the accuracy and convergence time even under moderate-to-strong scintillation. Cui et al.(2024) [31] found that during the February 2023 storm, PPP 3D RMS errors exceeded 0.5 m at over 80% of high-latitude stations, while equatorial stations showed milder degradation. The May 2024 extreme storm, the strongest of solar cycle 25, also showed severe impacts. Danilchuk et al. (2025) [32] reported auroral oval expansion to 30°N and PPP errors up to fivefold near the auroral boundaries. Bezerra et al. (2025) [33] observed 275% PPP error increases at high latitudes with multi-constellation benefits. Cappello et al. (2025) [34] documented increased cycle slips and phase residuals. Younas et al. (2025) [35] found mid-latitude PPP errors up to 70 m.

Despite these advances, most investigations target geodetic-grade dual-frequency receivers. The response of low-cost stations under extreme storms, especially when deployed as network master stations, remains underexplored. This paper addresses that gap by evaluating the May 2024 storm's impact on a low-cost GNSS station versus a nearby geodetic-grade station, analyzing both positioning performance and raw observation quality. The findings highlight the potential of low-cost devices as a cost-effective alternative for geodetic applications while identifying critical factors that may affect their reliability under adverse atmospheric conditions. The findings aim to inform future GNSS network designs and operational strategies, particularly in expanding accessibility to precise positioning in research, environmental monitoring, and various scientific fields. Ultimately, this work

supports the broader adoption of low-cost GNSS technology, advancing its application in networks where robustness and affordability are paramount.

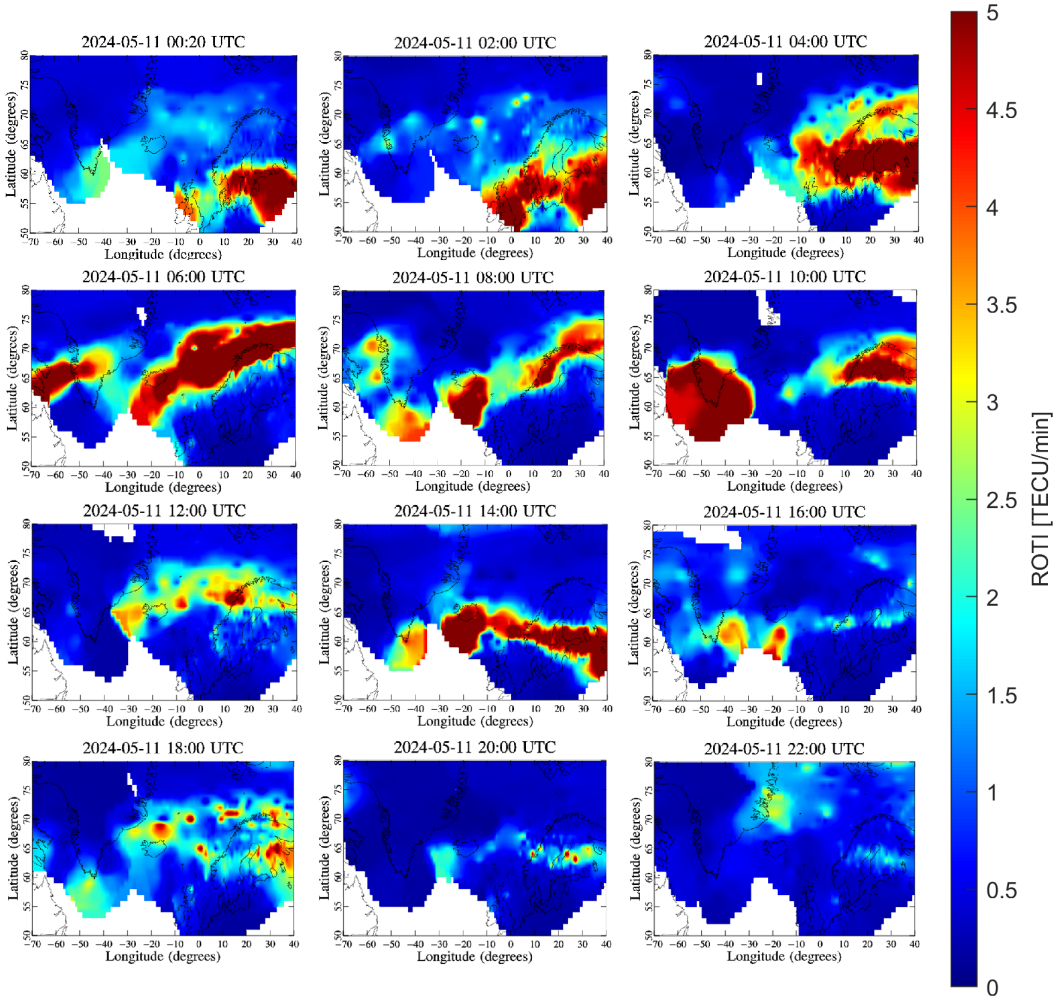


**Figure 2.** Sequence of regional ROTI maps over the European and Greenland sectors for 11 May 2024 at 2-h intervals, illustrating variations in ionospheric irregularity levels during a geomagnetic storm. Data was derived from GNSS observations provided by the Norwegian Mapping Authority (NMA).

## 2. Materials and Methods

To assess the impact of ionospheric disturbance events associated with the May 2024 geomagnetic storm on low-cost GNSS permanent stations, this study utilized observational data from the Centipede-RTK network. This network represents a newer generation of GNSS infrastructure using low-cost GNSS receivers and offering open-source services, making it particularly appealing for scientific research on geomagnetic effects. As of 2024, the network consists of approximately 700 continuously operating reference stations (CORSs) established by public institutions, private entities, and individuals worldwide. While the network's spatial density is highest in France, several stations are also scattered across Europe and other continents (Figure 3). The project has been supported since its inception in 2019 by the Institut national de la recherche agronomique (INRAE), along with contributions from research institutes, governmental bodies, and commercial partners.

Given that ionospheric scintillation and plasma irregularities predominantly occur at high latitudes—especially during geomagnetic storms—the geographic distribution of Centipede-RTK stations presents certain limitations for this type of analysis. The May 2024 storm, as discussed in the previous section, primarily affected auroral and subauroral regions (Figure 2). Consequently, among all Centipede-RTK stations with data availability

during the storm period, only the DYVA station—located in northern Norway—fell within the geomagnetically active region impacted by severe ionospheric disturbances. Thus, this station was selected for detailed analysis in this study due to both its high-latitude location and data availability throughout the geomagnetic storm period. To visualize and justify the selection of the DYVA station as the focus of this study, Figure 4 presents a dual-map illustration. The left side of the figure shows the geographical location of the DYVA low-cost GNSS station in central Norway, along with key surrounding European countries. As explained earlier, this station was selected from the Centipede-RTK network because of its high-latitude position and data availability during the major geomagnetic storm of 10–11 May 2024. Most Centipede stations are concentrated in France and other central European regions, which were less affected by the ionospheric disturbances during this event. DYVA, however, lies within the auroral zone, and it was exposed to significant ionospheric activity. The right side of Figure 4 shows the DYVA station superimposed on an ROTI map averaged over a two-hour period (3:00–5:00 a.m. UTC) on 11 May 2024. The elevated ROTI values (especially those exceeding 1.4 TECU/min in red and orange) highlight intense ionospheric irregularities. The DYVA station is located near the center of these disturbances, further supporting its relevance as a test site for evaluating GNSS performance under severe space weather conditions. Table 1 summarizes the technical specifications of the DYVA station, including its hardware configuration and geodetic coordinates.

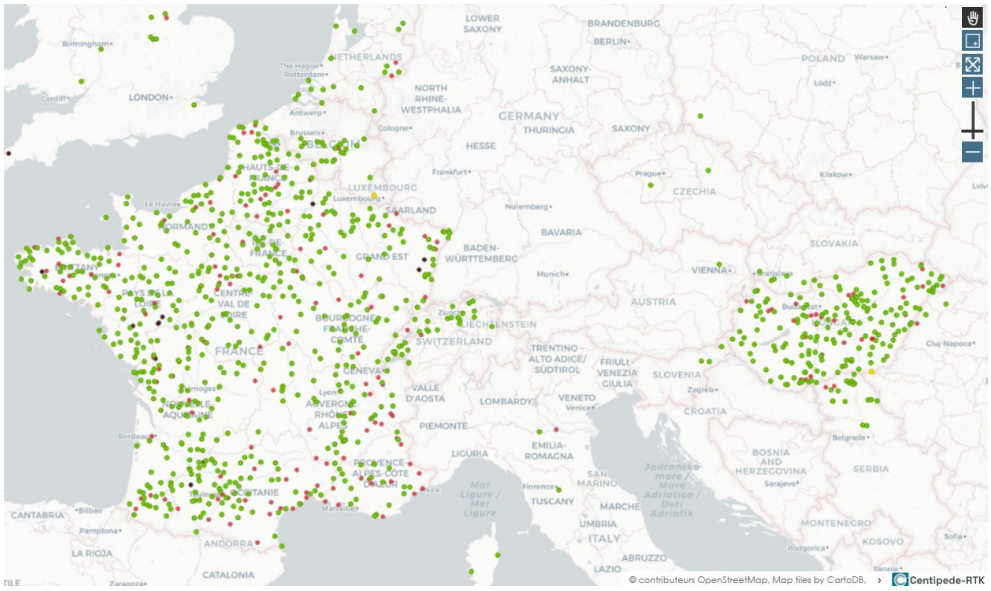


**Figure 3.** Centipede-RTK GNSS network map (https://centipede.fr/index.php/view/map/?repository=cent&project=centipede, accessed on 21 August 2025) considering a subset area of the European continent).

To investigate the impact of geomagnetic storms on low-cost GNSS permanent stations, raw GNSS observation data was gathered during a seven-day interval from 8 May 2024 to 14 May 2024. This period was specifically selected to encompass the pre-storm, peak, and recovery stages of the geomagnetic storm, thereby providing a thorough dataset for evaluating the impact of geomagnetic disturbances on the operation of low-cost GNSS signals. Table 2 reports the corresponding day of year (DOY) values for the selected dates, which are used throughout the data processing and analysis sections.

To contextualize the storm's intensity, both the planetary Kp index and ionospheric TEC-related indicators were examined over the selected interval. As illustrated in Figure 1, a pronounced escalation in geomagnetic activity was observed on May 10 (DOY 131) and May 11 (DOY 132), corresponding to the peak of the storm, while May 8 (DOY 129) exhibited

the lowest geomagnetic activity levels, representative of quiet ionospheric conditions. This temporal contrast provides a compelling basis for a comparative analysis. Accordingly, May 8 (DOY 129) is designated as the reference day to benchmark the effects of geomagnetic disturbances observed during the storm's peak. Such an approach allows for isolating storm-induced anomalies in GNSS performance by contrasting them against calm space weather baselines.

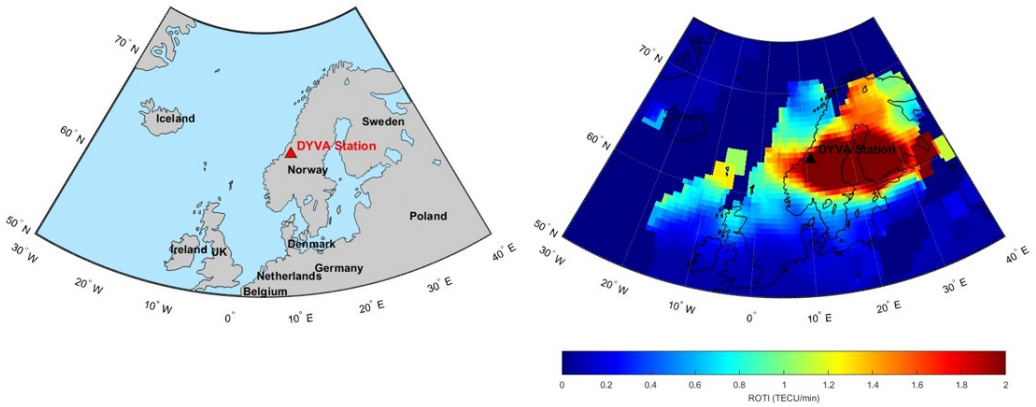


**Figure 4.** (**left**) Location of DYVA station and nearby European countries. (**right**) ROTI distribution on 11 May 2024 (averaged from 3:00 a.m. to 5:00 a.m. UTC), indicating intense ionospheric irregularities near the DYVA site.

**Table 1.** Technical specifications and geodetic information of the DYVA low-cost GNSS station selected from the Centipede-RTK network for ionospheric disturbances analysis.

| Station | Antenna | Receiver | Elevation (m) | Latitude | Longitude |
|---|---|---|---|---|---|
| DYVA | drotek DA910 | F9P drotek | 185.301 | 63.417094° | 10.966860° |

Note: Coordinate reference system is WGS84.

**Table 2.** Day of year (DOY) corresponding to the considered dates.

| Date | DOY |
|---|---|
| 8 May 2024 | 129 |
| 9 May 2024 | 130 |
| 10 May 2024 | 131 |
| 11 May 2024 | 132 |
| 12 May 2024 | 133 |
| 13 May 2024 | 134 |
| 14 May 2024 | 135 |

The methodology of this study is divided into two main components, each addressing a different aspect of how geomagnetic disturbances affect the performance of low-cost GNSS receivers.

The first part of the analysis focused on assessing the impact of ionospheric disturbances on positioning performance. To achieve this, PPP was carried out using data from the DYVA low-cost GNSS station during two selected days: one representing geomagnetically quiet conditions (DOY 129) and the other capturing the peak of a major geomagnetic storm (DOY 132). The analysis included full 24-h PPP solutions for both days, as well as a focused 1-h window (4:00–5:00 a.m. UTC), corresponding to the most disturbed period identified from tracking and ambiguity reset behavior. In addition to the DYVA station, PPP solutions were also computed for a nearby geodetic-grade station (TRDS00NOR) in order to provide a performance benchmark. Furthermore, a static relative positioning analysis

was conducted using TRDS00NOR as a reference base station, comparing single-frequency (L1) and dual-frequency (L1+L2) solutions under both quiet and storm-time conditions.

The second part of the analysis evaluated the effects of geomagnetic disturbances on raw GNSS observation quality. Specifically, detrended GPS L1 carrier-phase measurements were used to highlight discontinuities and noise in the signal, isolating the effects of ionospheric disturbances on phase tracking. The same 1-hour period used in the focused positioning analysis was selected for consistency. Additionally, signal-to-noise ratio (SNR) metrics and cycle slip occurrences were examined to quantify variations in signal strength and tracking reliability across both days.

Together, these two complementary analyses provided a comprehensive assessment of the impact of geomagnetic storm on low-cost GNSS performance, from raw signal behavior to final positioning accuracy.

*Software and Processing Tools*

Two open-source software tools were used in this study to analyze GNSS data: RTKLIB (available at https://www.rtklib.com/, accessed on 10 June 2025) and the Canadian Spatial Reference System Precise Point Positioning service (CSRS-PPP), an advanced online platform provided by Natural Resources Canada (https://webapp.csrs-scrs.nrcan-rncan.gc.ca/geod/tools-outils/ppp.php, accessed on 10 June 2025). RTKLIB was used to perform static relative positioning, while CSRS-PPP was used to carry out precise point positioning. Table 3 summarizes the key technical characteristics and processing configurations employed for both software tools.

**Table 3.** Comparison of capabilities of the software packages used in this study.

| Software | Version | Positioning Approach | Constellation | Frequency | Type of Observations | Reference Frame | Cutoff Angle |
|---|---|---|---|---|---|---|---|
| RTKLIB | demo5 | Static Relative Positioning | GPS, Galileo | L1, L2 | Code and Phase | ITRF2008 | 10 |
| CSRS-PPP | 3 | PPP Static | GPS, Galileo | L1, L2 | Code and Phase | ITRF2020 | 7.5 |

## 3. Results

This study investigates how geomagnetic storms and associated ionospheric disturbances influence the performance of low-cost GNSS permanent stations. Building on the context established in the previous sections—particularly the extreme space weather event observed on 11 May 2024 (DOY 132)—this analysis provides insights into the resilience and limitations of low-cost GNSS receivers when exposed to geomagnetic disturbances.

To quantify the storm's effects, GNSS data from the DYVA station in the Centipede-RTK network was analyzed, focusing on two representative days: DOY 132 (11 May 2024), corresponding to the peak of the geomagnetic storm, and DOY 129 (8 May 2024), identified as the quietest day in the selected period. By contrasting these two dates, this study evaluates the influence of ionospheric disturbances on both positioning performance, including relative and PPP techniques, and on the quality of raw GNSS observations.

### *3.1. Impact of Ionospheric Disturbances on Positioning Performance*

For the first part of the analysis, the impact of ionospheric disturbances on the performance of PPP solutions was assessed. Table 4 presents the root mean square (RMS) and maximum positioning errors obtained from the DYVA station over two 24-h periods. These days represent contrasting ionospheric conditions: DOY 129 (8 May 2024), a geomagnetically quiet day, and DOY 132 (11 May 2024), coinciding with the peak of the geomagnetic storm.

**Table 4.** RMS, standard deviation, and maximum positioning errors for DYVA station on DOYs 129 and 132.

| DOY | RMS [m] | | | | STD [m] | | | | MAX [m] | | | |
|---|---|---|---|---|---|---|---|---|---|---|---|---|
| | East | North | Up | 3D | East | North | Up | 3D | East | North | Up | 3D |
| 129 | 0.5043 | 0.6054 | 0.0486 | 0.7894 | 0.0234 | 0.0200 | 0.0474 | 0.0320 | 0.5769 | 1.2684 | 1.1986 | 1.6752 |
| 132 | 0.5123 | 0.6075 | 0.0598 | 0.7969 | 0.0696 | 0.0191 | 0.0597 | 0.0828 | 1.1641 | 2.6822 | 1.6495 | 3.1428 |

The results clearly show that geomagnetic activity degraded the positioning performance. On DOY 129, the PPP solution achieved relatively stable results, with a 3D RMS error of approximately 0.79 m and a maximum 3D error of 1.67 m. Conversely, DOY 132 displayed a comparable RMS error; however, as the max 3D error increased markedly to over 3.14 m. The RMS errors in the east and north components remained relatively stable between DOY 129 and DOY 132, suggesting that the average horizontal positioning accuracy was not drastically affected by the storm. However, the maximum error values revealed a more pronounced sensitivity to geomagnetic disturbances. The north component, for example, showed an increase in maximum error from 1.2684 m on the quiet day (DOY 129) to 2.6822 m on the storm day (DOY 132), more than doubling. The east component followed a similar trend, increasing from 0.5769 m to 1.1641 m. The up component exhibited both elevated RMS and maximum errors during the storm, with the maximum reaching 1.6495 m, compared with 1.1986 m on the quiet day. These results underscore the vulnerability of vertical positioning to ionospheric disturbances. This comparison highlights the susceptibility of low-cost GNSS PPP solutions to space weather effects and underlines the importance of further examining both the temporal characteristics of such degradations and their implications for high-accuracy applications. To further investigate the underlying causes of degraded PPP performance during storm-time conditions, Figures 5 and 6 illustrate the number of tracked satellites and the percentage of reset ambiguities throughout the day for both DOYs. These metrics are essential in assessing signal continuity and ambiguity resolution reliability.

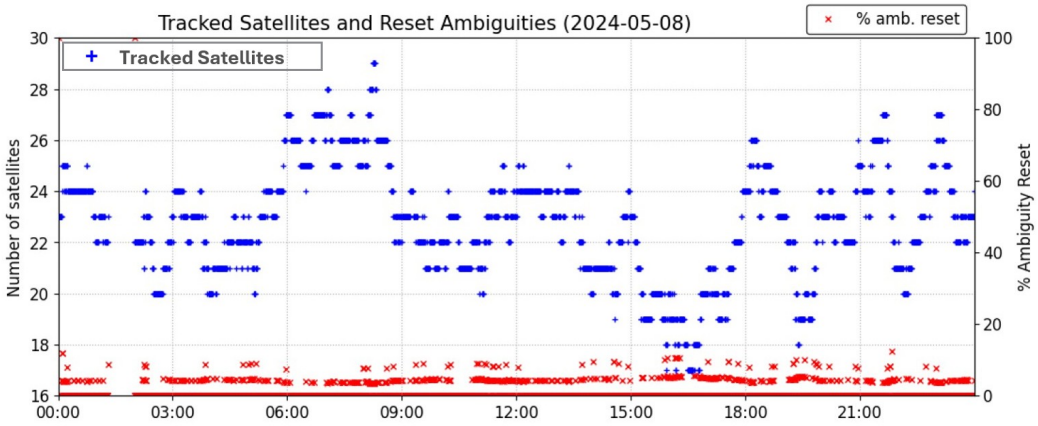


**Figure 5.** Tracked satellites and percentage of ambiguity resets for DYVA station on DOY 129.

Under quiet ionospheric conditions on DOY 129, the number of tracked satellites remained relatively stable throughout the day, generally ranging between 20 and 26. This steady satellite visibility reflects consistent tracking performance and minimal signal degradation. The percentage of ambiguity resets was also notably low, with most values remaining under 10%, indicating reliable carrier-phase tracking during a full day. In contrast, DOY 132—the peak of the geomagnetic storm—exhibited a markedly different behavior. Although the number of tracked satellites remained in a similar range (20–26), there were noticeably sharper and more frequent drops in visibility, particularly during two key in-

tervals: between 3:00 a.m. and 7:00 a.m. UTC and again from 4:00 p.m. to 8:00 p.m. UTC. These reductions suggest temporary losses of satellite lock, most likely due to ionospheric scintillation disrupting signal propagation. The impact is even more evident in the ambiguity reset data; multiple large spikes were observed, especially in the aforementioned intervals, with reset percentages reaching as high as 30–50%. This indicates substantial phase instability, an indicator of ionospheric disturbances.

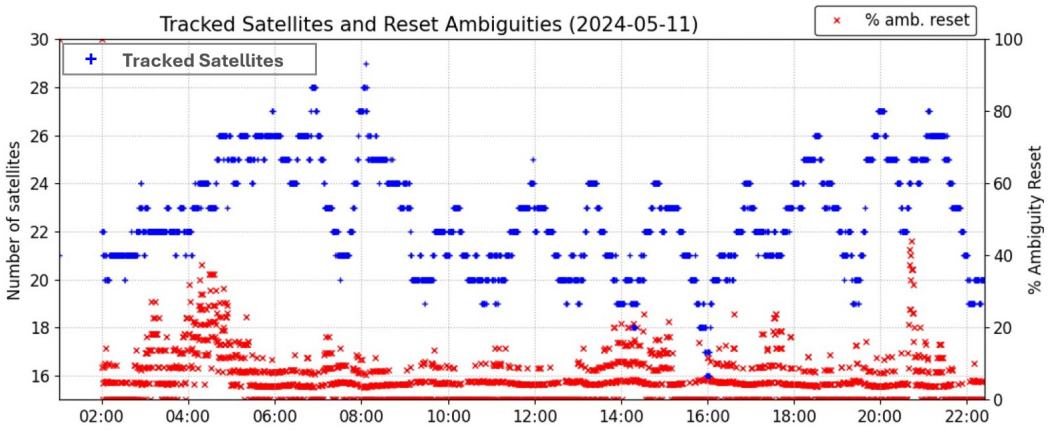


**Figure 6.** Tracked satellites and percentage of ambiguity resets for DYVA station on DOY 132.

Given the strong fluctuations and severe signal degradation observed at about 4:00–5:00 a.m. UTC, when the ambiguity resets peaked, this one-hour interval was selected as the focus for further analysis in the following sections. This targeted approach allowed for a more detailed assessment of positioning performance and observation quality during the period of the greatest disturbances.

To further examine the impact of the geomagnetic storm during its most active phase, PPP analysis was repeated for the one-hour interval between 4:00 a.m. and 5:00 a.m. UTC on both DOY 129 and DOY 132. This window was selected based on the previous analysis, which identified it as the period with the highest ambiguity reset percentages and strongest signal degradation.

Figures 7 and 8 show the PPP positioning results during this one-hour interval for the DYVA station. The figures display the estimated positions in latitude, longitude, and height, overlaid with their corresponding formal sigmas from the PPP solution. These plots enable a visual inspection of the convergence behavior and positioning stability under both quiet and disturbed ionospheric conditions.

For the latitude component ,DOY 132 started with initial errors close to 0.75 m and converged within the first 10–15 min, stabilizing around 0.4–0.45 m, with only minor fluctuations thereafter. DOY 129 began with larger initial errors (above 1.5 m) but converged to its stable value (near 1.1–1.2 m) in slightly less time. In the longitude (east) component, DOY 129 performed better. It converged quickly to a stable value of about –0.35 m with little variation. On DOY 132, the initial errors were larger (around 0.8 m), and the solution stabilized later, with a final value near –0.9 m. There was also more fluctuation during the convergence phase. The up component showed the slowest and least accurate convergence on both days. On DOY 129, the error started around 2.8 m and stabilized near 2.8 m with relatively smooth behavior. On DOY 132, the error was larger and took longer to settle, reaching a final value close to 3.5 m, with continued small variations throughout the hour. This is consistent with the general observation that vertical positioning is more sensitive to noise and atmospheric effects. In terms of overall performance, DOY 132 showed slower convergence in all three components compared with DOY 129, requiring more time to reach stable values. Nevertheless, in the latitude component, DOY 132 achieved a lower final

error than DOY 129. In contrast, both the longitude and height components converged more smoothly and to a better accuracy on DOY 129.

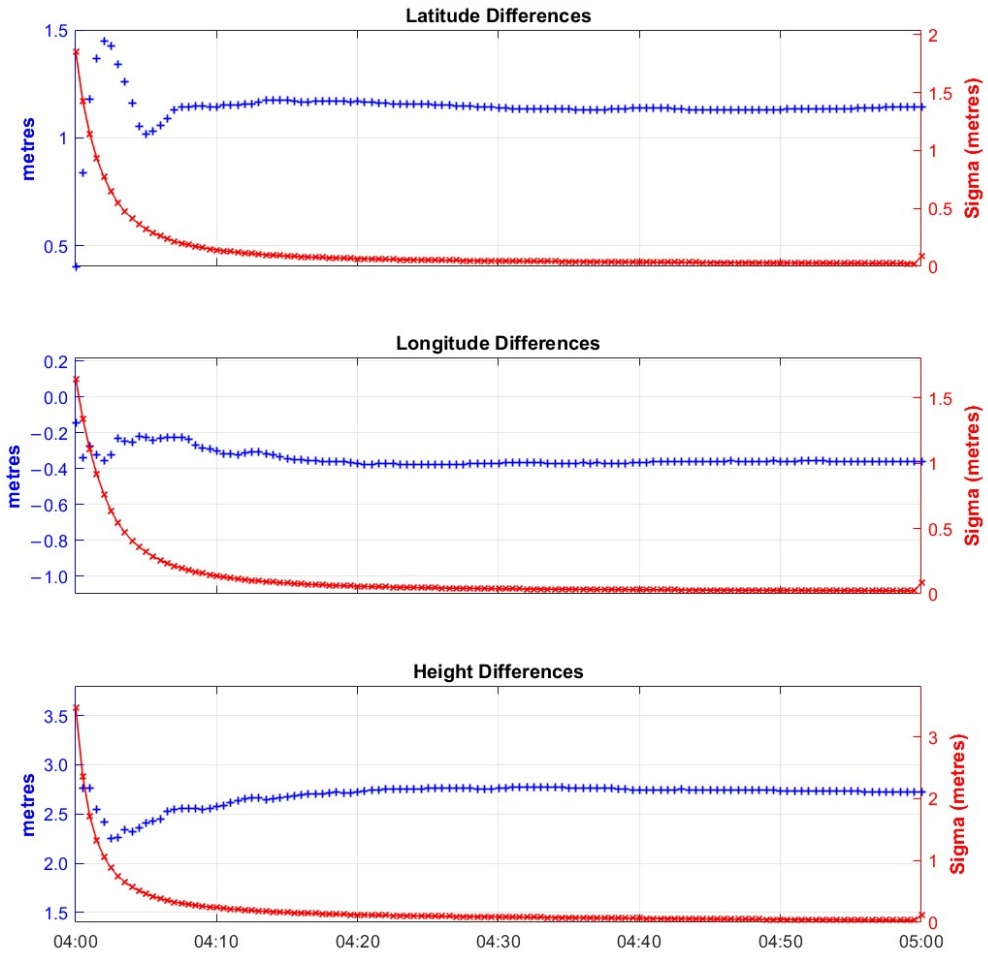


**Figure 7.** PPP positioning solution from 4:00 a.m. to 5:00 a.m. UTC on DOY 129. Blue points show deviations from the a priori position, and the red line shows the PPP standard deviations (95%).

Table 5 summarizes the RMS and maximum positioning errors computed during this one-hour interval for both days. The statistics reveal clear differences in behavior between storm and quiet conditions. The RMS errors showed higher values in all components for DOY 132, and the maximum positioning errors—particularly in the east and up components—were significantly higher during the storm period (DOY 132). For example, the maximum up error on DOY 132 reached 3.39 m, compared with 2.68 m on DOY 129. The east and north components also showed higher deviations, indicating degraded positioning stability under disturbed ionospheric conditions, even within a short time frame.

In addition to evaluating the impact of the geomagnetic storm on the low-cost DYVA station, a comparative analysis was conducted using a geodetic-grade reference station from the EUREF Permanent GNSS Network. The selected station, TRDS00NOR, is located in Trondheim, Norway, geographically close to DYVA but equipped with higher-grade instrumentation and situated at a slightly higher latitude. By applying the same PPP processing methodology to TRDS00NOR for DOY 132, this comparison allowed us to examine how ionospheric disturbances affected a geodetic receiver under the same geomagnetic disturbance. This comparison aimed to strengthen the overall analysis by providing a reference scenario. It allows for a more comprehensive understanding of how different classes of GNSS receivers respond to space weather disturbances under similar environmental and temporal conditions.

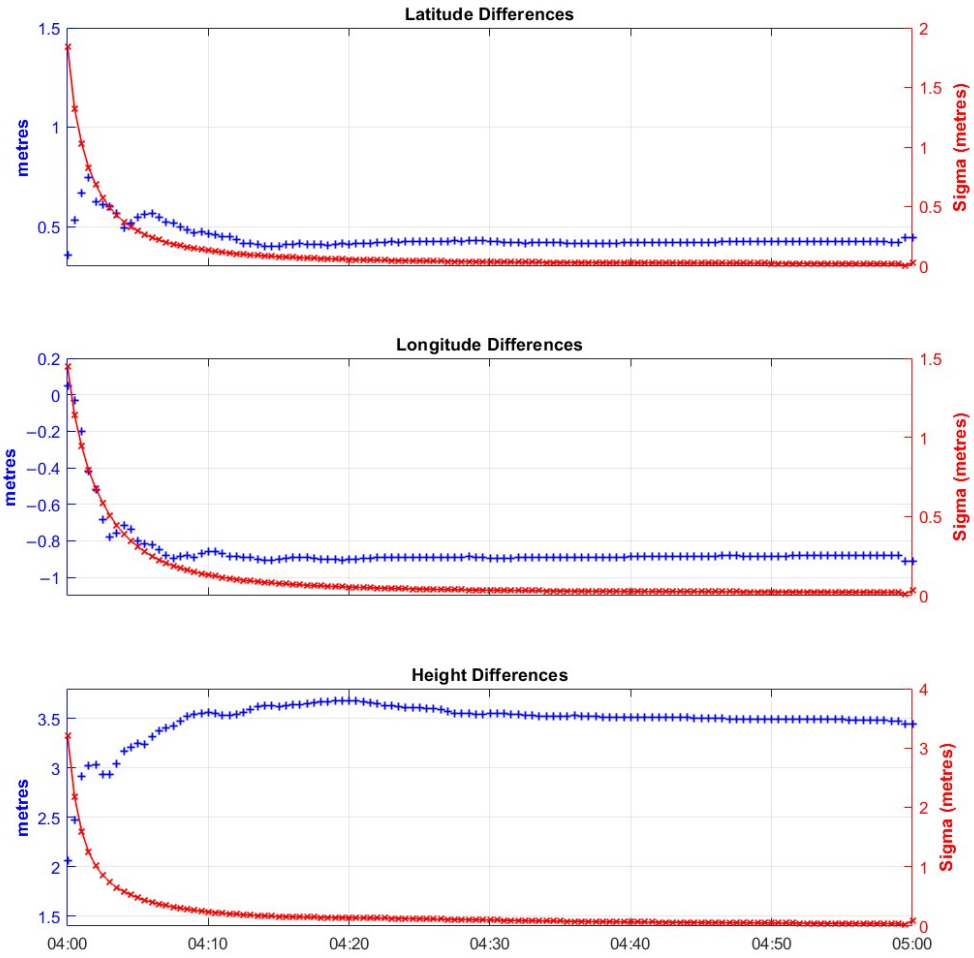


**Figure 8.** PPP positioning solution from 4:00 a.m. to 5:00 a.m. UTC on DOY 132. Blue points show deviations from the a priori position, and the red line shows the PPP standard deviations (95%).

**Table 5.** RMS and maximum positioning errors for DOYs 129 and 132, limited to the 4:00–5:00 a.m. UTC interval.

| DOY | RMS [m] | | | | MAX [m] | | | |
|---|---|---|---|---|---|---|---|---|
| | East | North | Up | 3D | East | North | Up | 3D |
| 129 | 0.5435 | 0.5872 | 0.2924 | 0.8518 | 0.8810 | 0.8884 | 2.6816 | 2.8775 |
| 132 | 0.5725 | 0.6011 | 0.3857 | 0.9153 | 1.4419 | 0.9035 | 3.3934 | 3.6714 |

As Table 6 illustrates, the RMS errors for the TRDS station remained below 0.6 m for all components, with a maximum 3D error of 2.90 m. These results demonstrate the robustness and stability of geodetic-grade receivers under disturbed ionospheric conditions. When compared with the low-cost DYVA station (Table 5), the high-grade system showed lower errors, particularly in the north and up components, and in terms of max errors, the TRDS station had a significantly lower max 3D error. This contrast not only validates the impact of equipment quality during space weather events but also strengthens the interpretation of DYVA's performance by establishing a reliable upper benchmark.

To further investigate positioning performance under disturbed conditions—and to leverage the proximity of TRDS00NOR—a relative positioning approach was carried out, using TRDS as the base station. This technique allowed for mitigation of common-mode errors, such as ionospheric and satellite orbit biases, offering an additional perspective on how storm-time conditions influence short-baseline GNSS solutions. This approach allowed assessment of the positioning accuracy under both quiet and disturbed ionospheric

conditions using single-frequency (L1) and dual-frequency (L1+L2) observations. Table 7 presents the RMS and standard deviation values for each coordinate component.

**Table 6.** RMS and maximum positioning errors for TRDS00NOR station, limited to the 4:00–05:00 a.m. UTC interval.

| DOY | RMS [m] | | | | MAX [m] | | | |
|---|---|---|---|---|---|---|---|---|
| | East | North | Up | 3D | East | North | Up | 3D |
| 129 | 0.6164 | 0.4830 | 0.1437 | 0.7962 | 0.6597 | 0.5545 | 1.2600 | 1.3358 |
| 132 | 0.6031 | 0.4987 | 0.3363 | 0.8518 | 1.0032 | 1.0352 | 2.6676 | 2.8964 |

**Table 7.** RMS and standard deviation of static relative positioning errors for DOYs 129 and 132 using L1 and L1+L2 observations.

| DOY | L1 | | | | | | L1+L2 | | | | | |
|---|---|---|---|---|---|---|---|---|---|---|---|---|
| | STD [m] | | | RMS [m] | | | STD [m] | | | RMS [m] | | |
| | East | North | Up | East | North | Up | East | North | Up | East | North | Up |
| 129 | 0.119 | 0.122 | 0.226 | 0.122 | 0.130 | 5.851 | 0.073 | 0.139 | 0.254 | 0.076 | 0.147 | 5.651 |
| 132 | 1.746 | 5.586 | 6.216 | 1.829 | 5.636 | 8.482 | 0.100 | 0.159 | 0.429 | 0.153 | 0.169 | 6.062 |

As shown in the table, the positioning performance on DOY 129 was generally consistent and accurate across both frequency modes. However, a substantial degradation was evident on DOY 132 when only L1 observations were used, especially in the north and up components, where the RMS errors rose to 5.6 m and 8.5 m, respectively. This contrast highlights the vulnerability of single-frequency processing under disturbed ionospheric conditions. When using dual-frequency (L1+L2) data on the same day, the positioning accuracy significantly improved across all components. The north RMS error, for example, dropped from 5.6 m to 0.17 m, and the up RMS decreased from 8.5 m to 6.1 m.

This improvement can be attributed to the use of the ionosphere-free (IF) linear combination in dual-frequency processing, which effectively eliminated the first-order ionospheric delay. As discussed earlier in the Introduction section, this approach is particularly beneficial during periods of heightened ionospheric activity, such as those caused by geomagnetic storms. Therefore, these results reinforce the critical role of dual-frequency observations in mitigating ionospheric errors and ensuring robust relative positioning under space weather disturbances.

### *3.2. Impact of Ionospheric Disturbances on Raw GNSS Observations*

Following the analysis of positioning performance, this subsection investigates how the geomagnetic storm of 10–11 May 2024 influenced the quality of the raw GNSS measurements. While the previous section focused on the positioning domain, this part shifts attention to the underlying observation data to better understand the extent of ionospheric disturbance effects on satellite signals.

To evaluate the signal quality degradation, carrier-phase measurements from all visible satellites were examined for both DOY 129 and DOY 132. A detrending approach was applied to the carrier-phase data in order to eliminate higher-order trends and emphasize measurement noise and discontinuities, which were obtained through second-order differentiation [36,37]. The analysis was constrained to the same one-hour interval (4:00–05:00 a.m. UTC) used in the positioning evaluation, ensuring consistency across both assessments. The x axis of the resulting plots corresponds to the epoch number, with each epoch representing a 30-second interval. The detrended carrier-phase measurements were derived from GPS L1 signals, which are universally available across all GPS satellites and commonly used in low-cost GNSS receivers.

As illustrated in Figures 9 and 10, the impact of the geomagnetic storm was clearly reflected in the behavior of the carrier-phase signals. On DOY 129, the detrended carrier phase appeared stable and continuous across all epochs, indicating clean signal reception with minimal phase noise. In contrast, DOY 132 revealed significant disruptions, with clear discontinuities and suspected cycle slips occurring around epochs 19–21. These abrupt deviations suggest a temporary loss of phase lock or increased noise due to ionospheric irregularities affecting signal propagation. After these anomalies, the receiver appeared to re-establish lock, but the data quality remained degraded relative to the quiet day. In terms of signal quality, the signal-to-noise ratio (SNR) for satellites located in the northwest sky region was found to decrease by up to approximately 13% on DOY 132 compared with DOY 129, indicating a noticeable reduction in signal quality during the storm. Additionally, there was an observed 5% increase in cycle slips on DOY 132 relative to DOY 129, further confirming the elevated phase instability induced by the geomagnetic activity.

This comparative analysis underscores the impact of ionospheric disturbances during geomagnetic storms on raw measurements. Such deficiencies might directly affect the reliability of ambiguity resolution and thus the overall performance of high-precision GNSS applications.

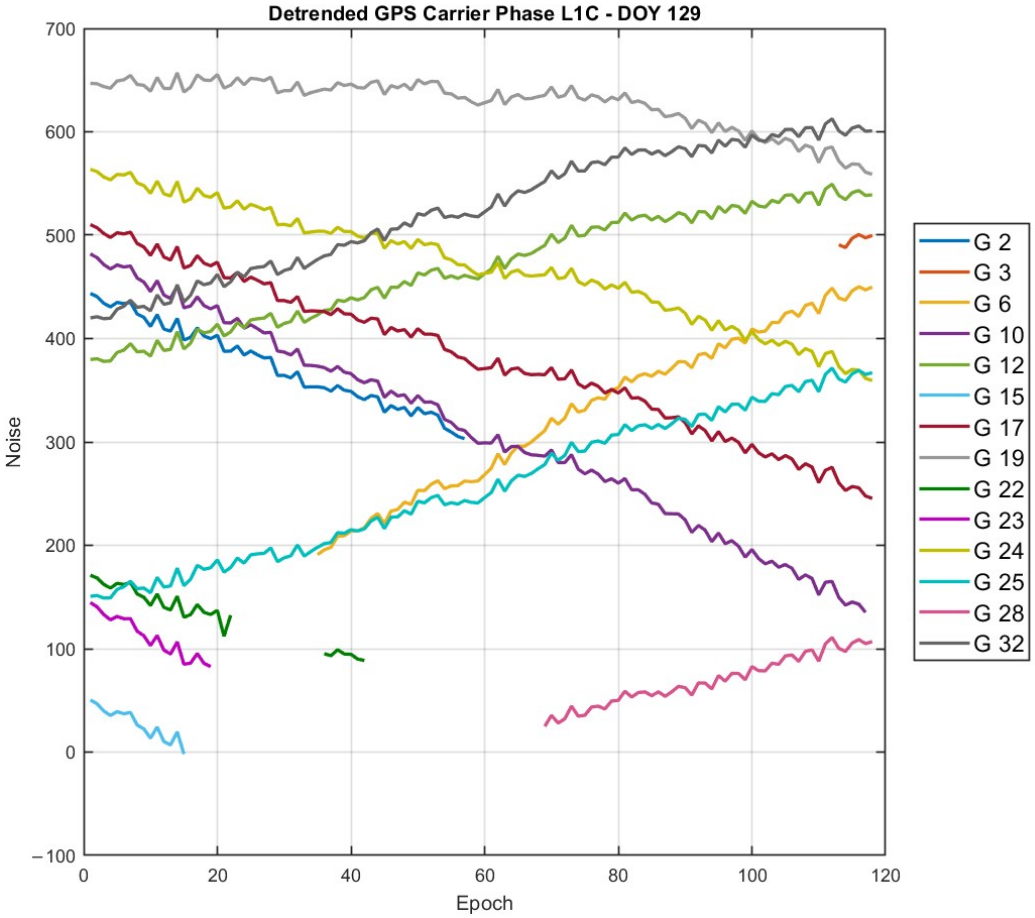


**Figure 9.** Detrended carrier phase residuals from 4:00 a.m. to 5:00 a.m. UTC on DOY 129.

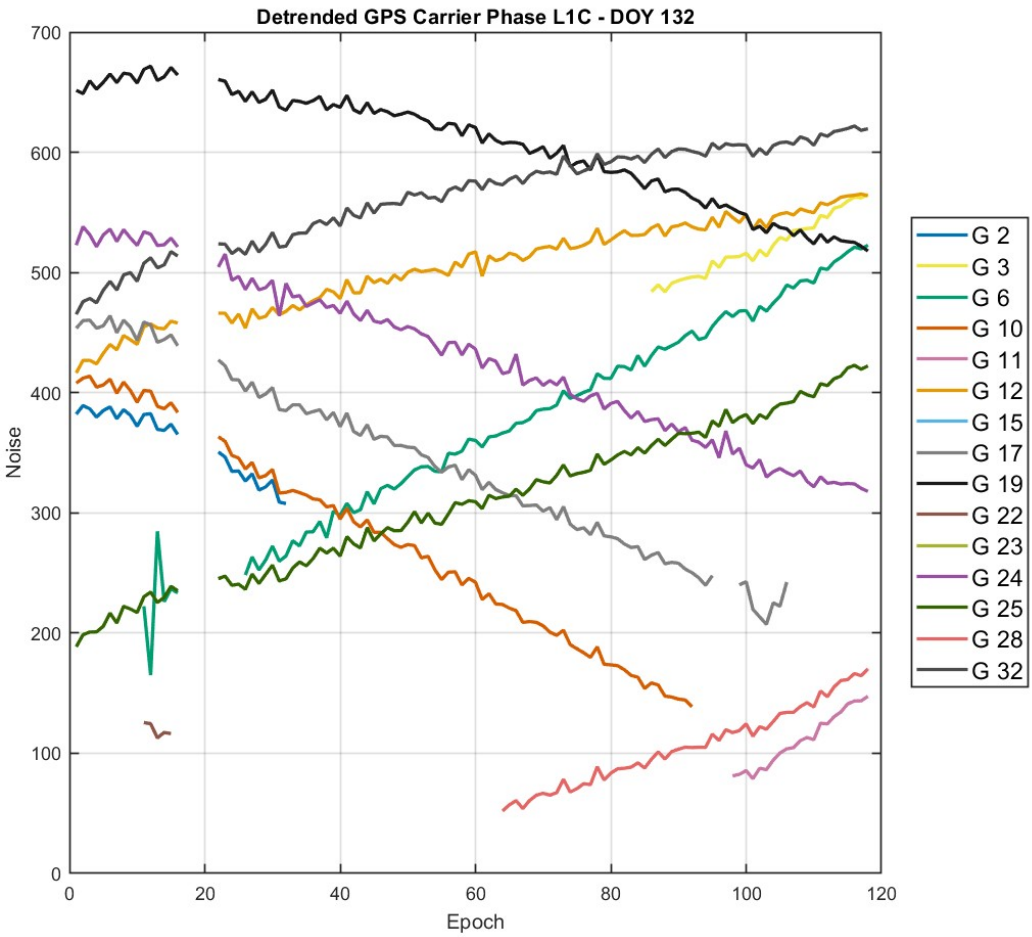


**Figure 10.** Detrended carrier phase residuals from 4:00 a.m. to 5:00 a.m. UTC on DOY 132.

## 4. Discussion

This study investigated the effects of ionospheric disturbances caused by a geomagnetic storm on the performance of a low-cost GNSS permanent station. The analysis was divided into two key parts: the impact on positioning performance and on raw GNSS observations.

As shown in the Results section, the first part of the analysis focused on evaluating positioning performance using PPP and relative positioning techniques. The comparison between the quiet day (DOY 129) and the storm day (DOY 132) revealed notable degradations during geomagnetic disturbances. The 24-h PPP results showed that while the RMS errors remained relatively stable, the maximum errors, particularly in the north and up components, increased significantly on DOY 132 (Table 4), demonstrating that space weather events caused occasional yet significant positional discrepancies. Further investigation during the 4:00–5:00 a.m. UTC interval reveal that the period with peak disturbance demonstrated more detailed differences. The DYVA station exhibited slower convergence and higher variability in PPP solutions during the storm. For instance, the height component was especially impacted, with errors reaching up to 3.39 m on DOY 132 compared with 2.68 m on DOY 129. When compared with a nearby geodetic-grade station (TRDS00NOR), the low-cost receiver displayed higher positioning errors under the same storm conditions. This comparative approach emphasized the robustness of geodetic receivers and provided a benchmark to interpret the performance of the low-cost system under identical space weather conditions. In addition to PPP, relative positioning analysis was performed as a complementary assessment to further characterize the positioning behavior of the DYVA

station. By using TRDS00NOR as a base station, this approach allowed for a more comprehensive evaluation across different processing techniques and frequency configurations. The analysis revealed that on DOY 129, the positioning performance remained consistent between single-frequency (L1) and dual-frequency (L1+L2) processing. However, on DOY 132, substantial degradations were observed in the single-frequency solution, especially in the north and up components. This difference highlights the advantage of dual-frequency processing—through the ionospheric-free combination—in mitigating ionospheric delay during disturbed conditions. The results from relative positioning reinforced the PPP findings and illustrated the increased vulnerability of single-frequency solutions under space weather events.

The second part of the analysis addressed the quality of raw GNSS observations. Detrended GPS L1 carrier-phase data revealed a clear increase in noise and discontinuities during the storm day. In particular, DOY 132 showed pronounced cycle slips around epochs 19–21, suggesting disruptions in signal tracking due to ionospheric disturbances. This interpretation was further supported by reduced average signal-to-noise ratios (SNRs), with up to a 13% decline observed for satellites in the northwestern sky region on DOY 132 compared with DOY 129. Moreover, a 5% increase in cycle slips was recorded on the storm day, underscoring reduced signal stability and receiver performance. The geomagnetic and ionospheric disturbance patterns observed during the storm, such as the equatorward shift of the mid-latitude ionospheric trough (MIT) and pronounced TEC depletions reported by Paul et al. (2025) [38], are consistent with the signal degradation and positioning errors recorded at the DYVA station. This agreement supports the interpretation that large-scale ionospheric restructuring during the event was a key driver of the observed GNSS performance losses. These findings are in general agreement with those reported in [34], which evaluated the impact of the same geomagnetic storm on geodetic-class GNSS receivers and similarly observed increased signal degradation and phase instabilities.

Together, these results highlight the sensitivity of low-cost GNSS systems to ionospheric disturbances, particularly during geomagnetic storms. The alignment of raw observation degradation with increased positioning errors confirms the direct influence of ionospheric disturbances on high-accuracy GNSS applications.

These findings highlight the performance characteristics of low-cost GNSS receivers under severe ionospheric disturbances and quantitatively demonstrate the extent of positioning and signal degradation during the geomagnetic storm. By comparing a low-cost receiver (DYVA) with a nearby geodetic-grade station (TRDS00NOR), the analysis provides a valuable benchmark for understanding how such systems behave under identical space weather conditions. The results show that while the geodetic receivers maintained higher accuracy and stability, low-cost receivers can still deliver usable performance, particularly when supported by dual-frequency processing and relative positioning techniques.

## 5. Conclusions

This study quantified the impact of the May 2024 G4 geomagnetic storm on the positioning accuracy and signal quality of a low-cost GNSS permanent station in Norway. Compared with a quiet day, the 3D positioning error nearly doubled, and during a one-hour storm window, the maximum 3D positional deviation increased by roughly 30%, accompanied by slower convergence. Benchmarking against a nearby geodetic-grade station confirmed higher errors for the low-cost unit, but dual-frequency relative positioning significantly reduced the impact of ionospheric delay. Signal analysis revealed clear storm-related degradation; the SNR dropped by up to 13% for the northwestern satellite sectors, and cycle slips increased by 5%, consistent with ionospheric scintillation effects. These results align with previous findings for high-grade receivers and highlight that while low-cost systems

are more sensitive to space weather, they can still deliver robust performance when using dual-frequency processing or relative positioning. This provides a practical benchmark for deploying low-cost GNSS receivers in regions where geodetic-grade infrastructure is limited.

**Author Contributions:** Conceptualization, M.B. and P.D.; methodology, M.B. and P.D.; software, M.B.; validation, M.B. and P.D.; formal analysis, M.B.; investigation, M.B.; resources, P.D.; data curation, M.B.; writing—original draft preparation, M.B.; writing—review and editing, M.B. and P.D.; visualization, M.B.; supervision, P.D.; project administration, P.D.; funding acquisition, P.D. All authors have read and agreed to the published version of the manuscript.

**Funding:** The research activity was carried out within the SPACE IT UP! project founded by the Italian Space Agency's Call for "Space Activities" (topic 15), related to MUR call n°341 of 03/15/2022, for "Partnerships extended to universities, research centers, companies for the financing of basic research projects" (Prot. CI-2022-DSR-042 of 18 July 2022), financed by Decree of Award of the Italian Space Agency n. 53 of 01/26/2024 - CUP E53C24000300006, as well as "Earth Observation Fund—Financing from the Presidency of the Council of Ministers pursuant to Art. 1, paragraph 254, of law 160/2019. The reference year 2024". The authors gratefully acknowledge the financial support obtained.

**Data Availability Statement:** The original data presented in this study is openly available from the Centipede RTK network repository at https://renag.resif.fr/pub/centipede_30s/2024/, accessed on 10 June 2025.

**Conflicts of Interest:** The authors declare no conflicts of interest.

## References

1. Kintner, P.M.; Ledvina, B.M.; De Paula, E.R. GPS and Ionospheric Scintillations. *Space Weather* **2007**, *5*. [CrossRef]
2. Adebiyi, S.J.; Ikubanni, S.O.; Adebesin, B.O.; Joshua, B.W.; Adekoya, B.J. Variations of GPS-TEC at an African Low Latitude Station During Geomagnetic Disturbances. *Phys. Mem.-J. Theor. Appl. Phys.* **2019**, *1*, 113–125.
3. Teunissen, P.; Montenbruck, O. *Springer Handbook of Global Navigation Satellite Systems*; Springer: Cham, Switzerland, 2017.
4. Valdés-Abreu, J.; Díaz, M.; Báez, J.; Stable-Sánchez, Y. Effects of the 12 May 2021 Geomagnetic Storm on Georeferencing Precision. *Remote Sens.* **2022**, *14*, 38. [CrossRef]
5. Zhao, D.; Cui, S.; Zhang, X.; Li, L.; Sun, P.; Bian, C.; Ban, W.; Hancock, C.M.; Wang, Q.; Zhang, K. Analysis of global ionospheric scintillation and GPS positioning interference triggered by full-halo CME-driven geomagnetic storm: A case study. *Adv. Space Res.* **2024**, *74*, 2492–2509. [CrossRef]
6. Wang, Y.; Yuan, Y.; Li, M.; Zhang, T.; Geng, H.; Wang, G.; Wen, G. Effects of Strong Geomagnetic Storms on the Ionosphere and Degradation of Precise Point Positioning Accuracy during the 25th Solar Cycle Rising Phase: A Case Study. *Remote Sens.* **2023**, *15*, 5512. [CrossRef]
7. Dabove, P.; Linty, N.; Dovis, F. Analysis of Multi-Constellation GNSS PPP Solutions under Phase Scintillations at High Latitudes. *Appl. Geomat.* **2020**, *12*, 45–52. [CrossRef]
8. International GNSS Service (IGS). International GNSS Service (IGS). Available online: https://igs.org/ (accessed on 25 November 2024).
9. EPN Central Bureau. EUREF Permanent Network Central Bureau (EPN CB). Available online: https://www.epncb.oma.be/ (accessed on 25 November 2024).
10. Kenyeres, A.; Bellet, J.G.; Bruyninx, C.; Caporali, A.; De Doncker, F.; Droscak, B.; Duret, A.; Franke, P.; Georgiev, I.; Bingley, R.; Huisman, L. Regional integration of long-term national dense GNSS network solutions. *GPS Solut.* **2019**, *23*, 122. [CrossRef]
11. SPIN3 GNSS. Servizio di Posizionamento Interregionale GNSS. Available online: https://www.spingnss.it/ (accessed on 25 November 2024).
12. Liu, G.; Huang, G.; Xu, Y.; Ta, L.; Jing, C.; Cao, Y.; Wang, Z. Accuracy Evaluation and Analysis of GNSS Tropospheric Delay Inversion from Meteorological Reanalysis Data. *Remote Sens.* **2022**, *14*, 3434. [CrossRef]
13. Vaquero-Martínez, J.; Antón, M. Review on the Role of GNSS Meteorology in Monitoring Water Vapor for Atmospheric Physics. *Remote Sens.* **2021**, *13*, 2287. [CrossRef]
14. Bramanto, B.; Gumilar, I.; Sidiq, T.P.; Kuntjoro, W.; Tampubolon, D.A. Sensing of the atmospheric variation using Low Cost GNSS Receiver. *IOP Conf. Ser. Earth Environ. Sci.* **2018**, *149*, 012073. [CrossRef]
15. Romero-Andrade, R.; Trejo-Soto, M.E.; Vázquez-Ontiveros, J.R.; Hernández-Andrade, D.; Cabanillas-Zavala, J.L. Sampling Rate Impact on Precise Point Positioning with a Low-Cost GNSS Receiver. *Appl. Sci.* **2021**, *11*, 7669. [CrossRef]

16. Bosser, P.; Ancelin, J.; Métois, M.; Rolland, L.; Vidal, M. Water vapour monitoring over France using the low-cost GNSS collaborative network Centipede. In Proceedings of the EGU General Assembly 2023, Vienna, Austria, 23–28 April 2023; pp. EGU23–9059. [CrossRef]
17. Dabove, P.; Di Pietra, V. Towards the Use of Low-Cost GNSS Receivers for Permanent Networks in Precision Agriculture. In Proceedings of the 2022 IEEE Workshop on Metrology for Agriculture and Forestry (MetroAgriFor), Perugia, Italy, 3–5 November 2022; pp. 244–248.
18. Pira, A.; Ancelin, J.; Coulombier, T.; Dausse, D.; Ballu, V.; Testut, L.; Gaugue, A. Physalia: Plateforme HYdrographique pour la Surveillance Altimétrique du Littoral. *Lettre D'Information Résif* **2021**, *20*, 13–14.
19. Dabove, P.; Di Pietra, V. A Low-Cost Open-Source GNSS Network for Network Real-Time Kinematic Positioning: Which Future and Performances? In Proceedings of the 2023 IEEE/ION Position, Location and Navigation Symposium (PLANS), Monterey, CA, USA, 24–27 April 2023; pp. 272–279.
20. Dabove, P.; Di Pietra, V. A GNSS Low-Cost RTK Network: Positioning and Atmospheric Monitoring Performances in Mountain Areas. In Proceedings of the 2024 International Technical Meeting of The Institute of Navigation, Long Beach, CA, USA, 23–25 January 2024; pp. 858–868. [CrossRef]
21. Dabove, P.; Bagheri, M. Enhancing Atmospheric Monitoring Capabilities: A Comparison of Low- and High-Cost GNSS Networks for Tropospheric Estimations. *Remote Sens.* **2024**, *16*, 2223. [CrossRef]
22. Dabove, P.; Bagheri, M. Assessing Low-Cost GNSS Network Performance for Atmospheric and Positioning Applications: A Preliminary Multi-Station Analysis of a Low-Cost Network. In Proceedings of the 2025 IEEE/ION Position, Location and Navigation Symposium (PLANS), Salt Lake City, UT, USA, 28 April–1 May 2025; pp. 505–510. [CrossRef]
23. Skone, S.; Knudsen, K.; de Jong, M. Limitations in GPS receiver tracking performance under ionospheric scintillation conditions. *Phys. Chem. Earth Part A Solid Earth Geod.* **2001**, *26*, 613–621. [CrossRef]
24. Basu, S.; Basu, S.; Groves, K.M.; Yeh, H.C.; Su, S.Y.; Rich, F.J. A comparison of TEC fluctuations and scintillations at Ascension Island. *J. Atmos. Sol.-Terr. Phys.* **1999**, *61*, 1219–1226. [CrossRef]
25. Guo, K.; Vadakke Veettil, S.; Weaver, B.J.; Aquino, M. Mitigating high latitude ionospheric scintillation effects on GNSS Precise Point Positioning exploiting 1-s scintillation indices. *J. Geod.* **2021**, *95*, 30. [CrossRef]
26. Pi, X.; Mannucci, A.; Lindqwister, U.; Ho, C. Monitoring of global ionospheric irregularities using the worldwide GPS network. *Geophys. Res. Lett.* **1997**, *24*, 2283–2286. [CrossRef]
27. NOAA Space Weather Prediction Center. Planetary K-Index. Available online: https://www.swpc.noaa.gov/products/planetary-k-index (accessed on 25 November 2024).
28. Bartels, J. The Standardized Index Ks and the Planetary Index Kp. *Ann. Int. Géophysique (AIGY)* **1957**, *13*, 177–188.
29. Linty, N.; Minetto, A.; Dovis, F.; Spogli, L. Effects of Phase Scintillation on the GNSS Positioning Error During the September 2017 Storm at Svalbard. *Space Weather* **2018**, *16*, 1317–1329. [CrossRef]
30. Luo, X.; Gu, S.; Lou, Y.; Xiong, C.; Chen, B.; Jin, X. Assessing the Performance of GPS Precise Point Positioning Under Different Geomagnetic Storm Conditions During Solar Cycle 24. *Sensors* **2018**, *18*, 1784. [CrossRef]
31. Cui, S.; Zhang, X.; Zhao, D.; Ban, W.; Wang, Q.; Hancock, C. M.; Zhang, K. Assessment of Ionospheric Scintillation Effects on GPS PPP during the February 2023 Geomagnetic Storm. *J. Glob. Position. Syst.* **2024**, *19*, 24–35. Available online: https://www.cpgps.org/wwwroot/issue202403/2023_JoGPS_Vol19_pp24_35.pdf (accessed on 10 June 2025). [CrossRef]
32. Danilchuk, E.; Yasyukevich, Y.; Vesnin, A.; Klyusilov, A.; Zhang, B. Impact of the May 2024 Extreme Geomagnetic Storm on the Ionosphere and GNSS Positioning. *Remote Sens.* **2025**, *17*, 1492. [CrossRef]
33. dos Santos Bezerra, L.; de Oliveira, P.S.; Krueger, C.P. Performance analysis of multi-GNSS PPP under the effects of extreme geomagnetic event: A case study of Mother's Day solar storm (10–15 May 2024). *Adv. Space Res.* **2025**, *in press.* [CrossRef]
34. Cappello, G.; Gioia, C.; Angrisano, A.; Portelli, G.; Gaglione, S. The G4 Solar Storm of May 2024: Impact on the GNSS Carrier-Phase Measurements. In Proceedings of the ION Precise Time and Time Interval Meeting, Long Beach, CA, USA, 28 January 2025.
35. Younas, W.; Nishimura, Y.; Liao, W.; Semeter, J.L.; Mrak, S.; Morton, Y.J.; Groves, K.M. Spatio-Temporal Evolution of Mid-Latitude GPS Scintillation and Position Errors During the May 2024 Solar Storm. *J. Geophys. Res. Space Phys.* **2025**, *130*, e2025JA033839. [CrossRef]
36. Gogoi, N.; Minetto, A.; Linty, N.; Dovis, F. A Controlled-Environment Quality Assessment of Android GNSS Raw Measurements. *Electronics* **2019**, *8*, 5. [CrossRef]

37. Riley, S.; Landau, H.; Gomez, V.; Mishukova, N.; Lentz, W.; Clare, A. Positioning with Android GNSS Observables. *GPS World* **2018**, *29*, 18–34.
38. Paul, K.S.; Haralambous, H.; Moses, M.; Oikonomou, C.; Potirakis, S.M.; Bergeot, N.; Chevalier, J.M. Investigation of the Ionospheric Response on Mother's Day 2024 Geomagnetic Superstorm over the European Sector. *Atmosphere* **2025**, *16*, 180. [CrossRef]